nature structural & molecular biology

p53 pulses lead to distinct patterns of gene expression albeit similar DNA-binding dynamics

Antonina Hafner[1], Jacob Stewart-Ornstein[1], Jeremy E Purvis[2], William C Forrester[3], Martha L Bulyk[4,5] & Galit Lahav[1]

The dynamics of transcription factors play important roles in a variety of biological systems. However, the mechanisms by which these dynamics are decoded into different transcriptional responses are not well understood. Here we focus on the dynamics of the tumor-suppressor protein p53, which exhibits a series of pulses in response to DNA damage. We performed time course RNA sequencing (RNA-seq) and chromatin immunoprecipitation sequencing (ChIP-seq) measurements to determine how p53 oscillations are linked with gene expression genome wide. We discovered multiple distinct patterns of gene expression in response to p53 pulses. Surprisingly, p53-binding dynamics were uniform across all genomic loci, even for genes that exhibited distinct mRNA dynamics. Using a mathematical model, supported by additional experimental measurements in response to sustained p53 input, we determined that p53 binds to and activates transcription of its target genes uniformly, whereas post-transcriptional mechanisms are responsible for the differences in gene expression dynamics.

Many transcription factors are known to respond to multiple signals and activate various downstream programs[1–6]. Specificity between a particular input and output can be achieved through regulation of transcription factor abundance, post-translational modifications, or binding to cofactors. Another potential level of regulation is through the temporal dynamics of transcription factors. Indeed, recent single-cell studies point to a few examples in which the dynamics of transcription factors differ for different stimuli[5–7] and lead to distinct gene expression and phenotypic responses[3,8,9]. Understanding the molecular mechanisms that detect time-dependent features of transcription factors and decode them into distinct gene expression profiles remains a challenge. Here we focused on the dynamics of the tumor-suppressing transcription factor p53 and studied how its stereotypic pulses in response to DNA damage[10,11] affect the activation of its downstream target genes genome wide.

The tumor-suppressor protein p53 has a major role in the control of cell fate decisions. p53 is induced in response to stress and activates the transcription of ample stress-response genes. Several mechanisms of how p53 selectively activates target genes have been proposed. For example, a recent 'affinity model' suggests that p53's affinity to the promoters of cell-cycle-arrest genes is stronger than its affinity for the promoters of apoptotic genes. In this model, the choice between alternative downstream programs depends on the abundance of p53 (refs. 12–15). Specific post-translational modifications on p53 and interactions with specific cofactors have also been proposed to confer preference for some promoters over others[16–20]. In addition, the dynamics of p53 have recently been shown to play an important role in the response to DNA damage; different stimuli trigger different p53 dynamics, and p53 dynamics were suggested to carry information that affect gene expression and cell fate[3,4,7,10]. However, recent ChIP-seq studies showed substantial overlap between the strongly bound p53 regions independent of the treatment or cell line[21,22]. The results from these studies challenge the idea of context-specific regulation by p53 and re-pose the demand to further understand how different regulations of p53 control the induction of its target genes.

Here we studied how p53 dynamics are linked with gene expression. Recent studies have looked at the response of a few known p53 target genes to double-strand-break-induced p53 pulses and found that not all the tested genes showed a response, and that among the responders, there was diversity in the dynamics and amplitudes of expression[3,23]. The stability of mRNA was suggested to correlate with the differences in dynamic behavior between the tested genes[23,24]. However, the specific role of p53 dynamics in regulating the expression of genes across the genome, and the relationship between p53 dynamics and binding to its direct targets, has not been explored. In this work, we used RNA-seq to measure global gene expression in response to p53 pulses, allowing us to quantify the dynamics of p53's downstream target genes in an unbiased way across the genome. We compared our findings in p53 wild-type cells with those in cells expressing p53 shRNA and focused on the p53-dependent genes. We also performed ChIP-seq to identify direct targets of p53. Our genome-wide quantitative dynamical data allowed us to identify p53-dependent target genes, to determine the specific parameters describing their kinetics,

[1]Department of Systems Biology, Harvard Medical School, Boston, Massachusetts, USA. [2]Department of Genetics, University of North Carolina at Chapel Hill, Chapel Hill, North Carolina, USA. [3]Developmental and Molecular Pathways, Novartis Institutes for Biomedical Research, Cambridge, Massachusetts, USA. [4]Division of Genetics, Department of Medicine, Brigham and Women's Hospital and Harvard Medical School, Boston, Massachusetts, USA. [5]Department of Pathology, Brigham and Women's Hospital and Harvard Medical School, Boston, Massachusetts, USA. Correspondence should be addressed to G.L. (Galit_Lahav@hms.harvard.edu).

Received 17 February; accepted 20 July; published online 21 August 2017; doi:10.1038/nsmb.3452

and to develop a quantitative model that captures these dynamics and predicts the response under a new p53 dynamical input.

RESULTS

p53 oscillations lead to multiple patterns of gene expression

To establish a comprehensive connection between p53 dynamics and gene expression, we focused on the response to DNA damage caused by γ-irradiation, which triggers stereotypic p53 pulses[10,11,25] (**Fig. 1a**). We measured gene expression by mRNA-seq every hour during the first two pulses (12 h) and again at 24 h. Our analysis revealed 229 differentially expressed genes with at least a two-fold change in expression relative to the basal condition at one or more time points (FDR < 0.2, *t* test, Benjamini–Hochberg corrected). We clustered these genes based on their normalized expression within the first 12 h (*z* scores) and defined five main dynamical patterns (**Fig. 1b**,**c**), including three activated and two repressed clusters (**Supplementary Data Set 1**).

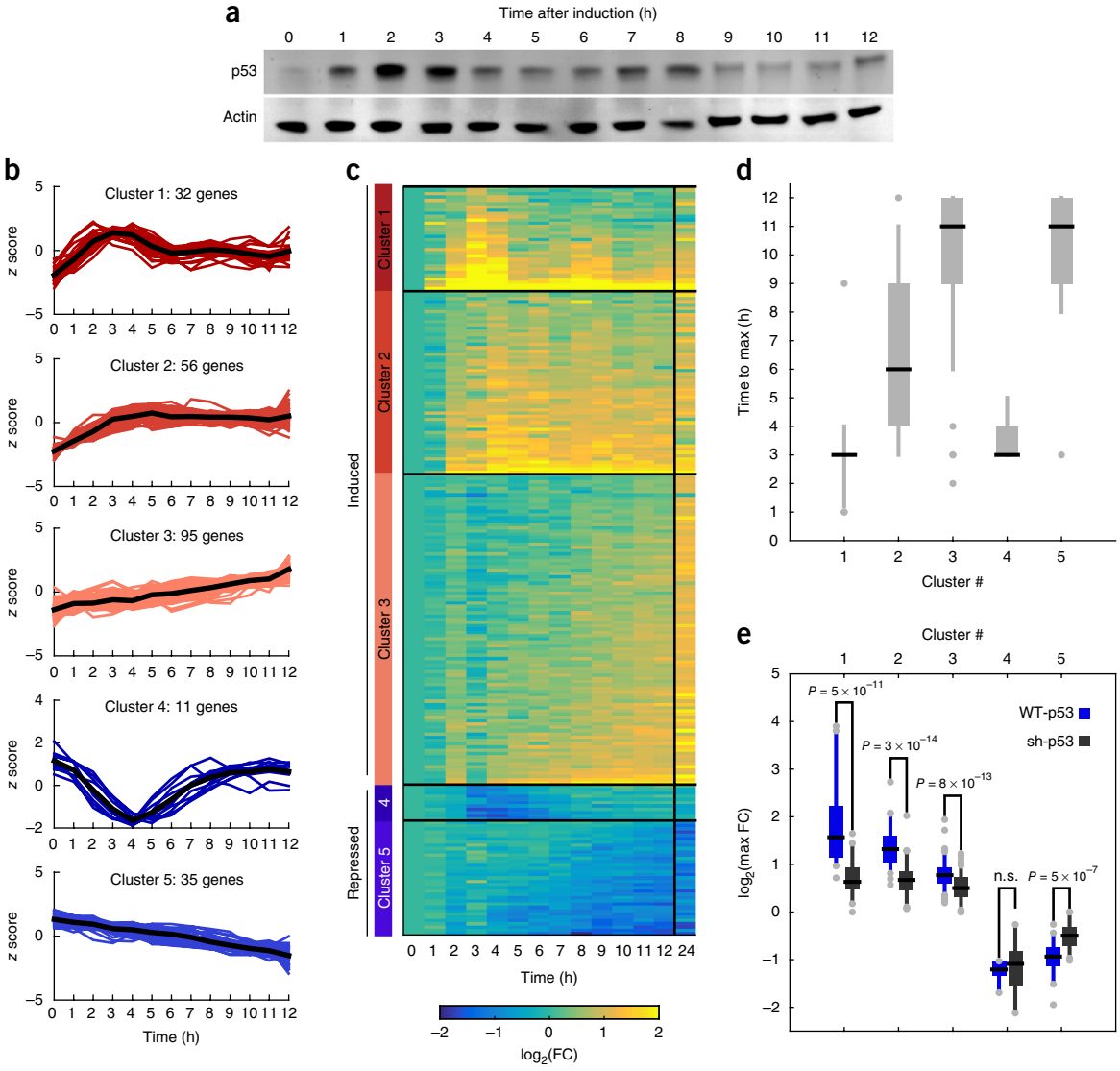

Figure 1 Time course mRNA-seq reveals distinct clusters of gene expression dynamics in response to γ-irradiation. (**a**) Western Blot for p53, with actin as a control, following 10 Gy γ-irradiation, representative of three independent experiments. Samples were taken every hour for the first 12 h, during which the p53 protein undergoes two pulses. Note that while p53 pulses in individual cells are not damped, at the population level they appear damped owing to the loss of synchrony between cells[10,11,25]. Uncropped gel images are shown in **Supplementary Data Set 5**. (**b**) Genome-wide expression profiling following γ-irradiation. Samples were taken every hour for the first 12 h, as well as 24 h post irradiation. 229 genes were found to be differentially expressed relative to the basal level. Differential expression was defined as fold change > 2 and FDR < 0.2 (*t* test, Benjamini–Hochberg corrected) based on two independent experiments. Clustering was based on normalized time trace for each gene (*z* score) into five expression clusters, three induced (red) and two repressed (blue). Mean expressions of each cluster are shown in black. (**c**) Heat map of the clustered genes. Clusters are ordered based on the median activation time (shown in **d**). (**d**) The distribution of times to reach the maximal fold change per cluster. Black lines indicate the median, and the box edges and whiskers extend to the 25–75% and the 5–95% quantiles, respectively. (**e**) Distributions of maximal $\log_2$ (fold change) in the first 10 h post irradiation per cluster for p53 wild type cells (blue, WT-p53) and p53 knockdown cells (gray, sh-p53). FC, fold change. Box edges represent the interquartile range, black midlines indicate the median, and the lower and upper whiskers extend to the 5th and 95th percentiles, respectively. *P* values were calculated using a two-sided *t* test. Individual dots represent outliers. n.s., not significant.

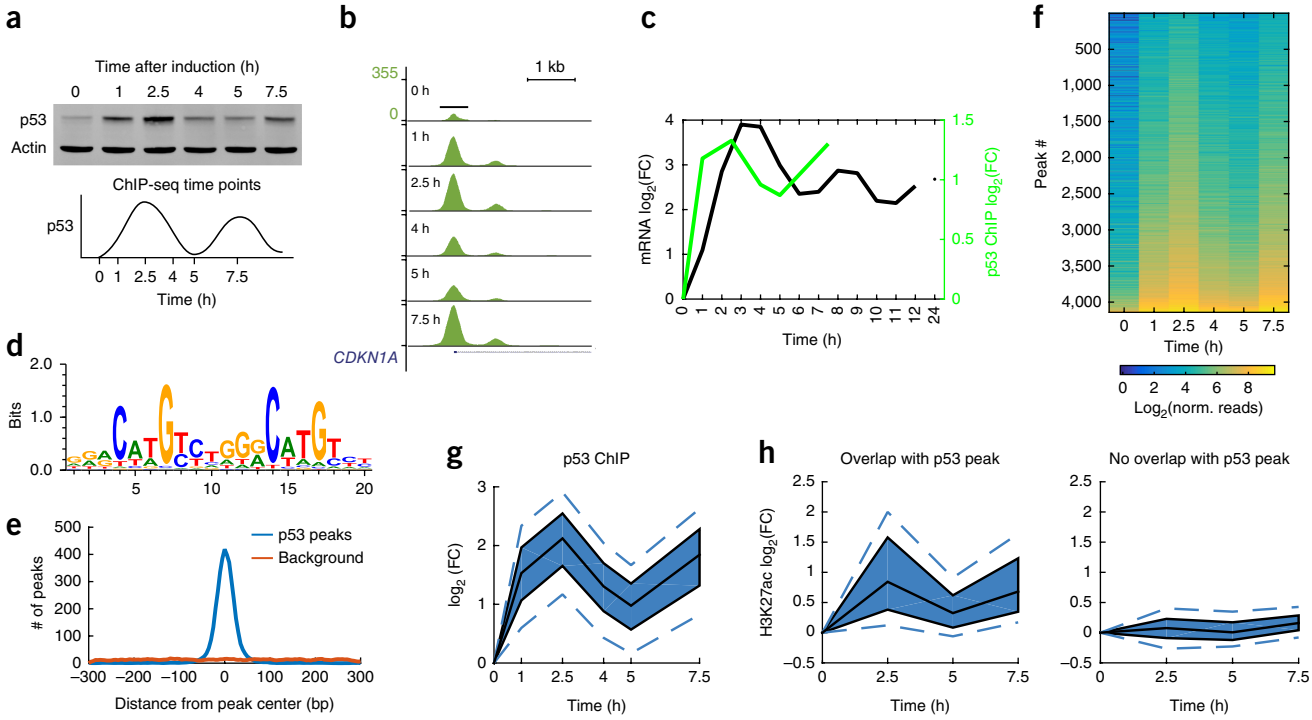

Figure 2 Time course p53 ChIP-seq experiment shows pulsatile dynamics genome wide. (**a**) Western blot of p53 protein levels, with actin as a control, at the selected time points for the ChIP-seq experiment sampling the first two p53 pulses (uncropped gel image in **Supplementary Data Set 5**). (**b**) p53 ChIP peak at the *CDKN1A* promoter with signal normalized to the total number of reads in each sample (UCSC tracks generated by HOMER software). (**c**) Quantification of the $\log_2$(FC) of p53 ChIP peak in **b** plotted with p21 mRNA dynamics from the mRNA-seq experiment. FC, fold change. (**d**) *De novo* motif found using the HOMER software present in 86.6% of the peaks (1.5% of background genomic regions) and plotted using WebLogo. (**e**) Distribution of motif (from **d**) start positions relative to the p53 peak centers. (**f**) Heat map of normalized reads in a total of 4141 p53 ChIP peaks, ordered by peak intensity. (**g**) Quantile plot of p53 ChIP peak $\log_2$(FC). The area shaded in dark blue represents the interquartile range, the black lines indicate the median, and the lower and upper dashed blue lines show the 10th and 90th percentiles, respectively. (**h**) H3K27ac ChIP was done at 0, 2.5, 5 and 7.5 h time points. Quantile plot shows H3K27ac ChIP peaks that overlap with the p53 ChIP peaks (left, 1,075 peaks) and of H3K27ac peaks that do not overlap with p53 (right, 26,153 peaks).

Cluster 1 included genes whose expression followed the p53 protein level and pulsed with an approximately 1-h delay (**Fig. 1c**,**d**). Cluster 2 included genes that were activated during the first 5 h and retained high expression levels throughout the time course. The genes in cluster 3 showed a slow continuous increase in expression throughout the time of measurement. Repressed genes were clustered on the basis of showing either transient repression (cluster 4) or continuous repression (cluster 5). To examine the dependence of these dynamical behaviors on p53, we performed a time course mRNA-seq in the same cell line expressing a p53 shRNA. We found that the fold changes of activation or repression of genes in clusters 1, 2, 3 and 5 were significantly attenuated in the p53 knockdown line (**Fig. 1e** and **Supplementary Fig. 1a**). Repressed genes in cluster 4 were not significantly affected under p53 knockdown, suggesting that their repression in response to irradiation is independent of p53 (**Fig. 1e** and **Supplementary Fig. 1a**). The reverse approach (first eliminating genes that were not affected by p53 shRNA and then clustering them) also led to the elimination of cluster 4, and the other clusters were largely unchanged (details and statistics in Online Methods).

The time it took each gene to reach a maximum fold change varied among the p53-dependent clusters. Among the activated genes, cluster 1 had the fastest induction time of 3 h. Cluster 2 showed an intermediate induction time with a median of 6 h. Genes in clusters 3 and 5 took 11 h to reach their maximal fold change (**Fig. 1d**). Cluster 1 had the highest fraction of literature-described p53 target genes (**Supplementary Fig. 1b**) and was enriched in Gene Ontology categories associated with DNA-damage response and the p53 signal-transduction pathway (**Supplementary Fig. 1c**). Known p53 target genes were also significantly enriched in clusters 2 and 3, although they represented a much lower fraction of the total genes in these groups (**Supplementary Fig. 1b**). Taken together, the results from our gene expression profiling analysis showed that γ-irradiation leads to five distinct patterns of mRNA dynamics, and four of these patterns (clusters 1, 2, 3 and 5) are p53 dependent.

Time course p53 ChIP-seq reveals pulsatile p53 DNA binding

To identify directly bound p53 genes and determine whether the distinct patterns of gene expression (**Fig. 1b**,**c**) result from differential binding of p53, we performed ChIP-seq of p53 during the first and second pulses following irradiation (**Fig. 2a**). We first looked at the well-established p53-binding site in the promoter of *CDKN1A*[26,27], a canonical p53 target gene from cluster 1 (**Fig. 2b**). We detected the expected promoter-proximal p53 ChIP peak (**Fig. 2b**) and a smaller adjacent peak that has also been seen in other p53 ChIP data sets[21,22,28]. Quantification of the stronger p53 ChIP peak after DNA damage revealed pulsatile binding dynamics, consistent with those of p53 protein levels and the pulses in *CDKN1A* mRNA level (**Fig. 2c**).

We next looked at p53 binding across the genome. We found a total of 4,141 peaks that were bound by p53 across all time points (**Supplementary Data Set 2**). The top *de novo* motif found corresponded to the known p53-binding site[26,29,30]. This motif was present

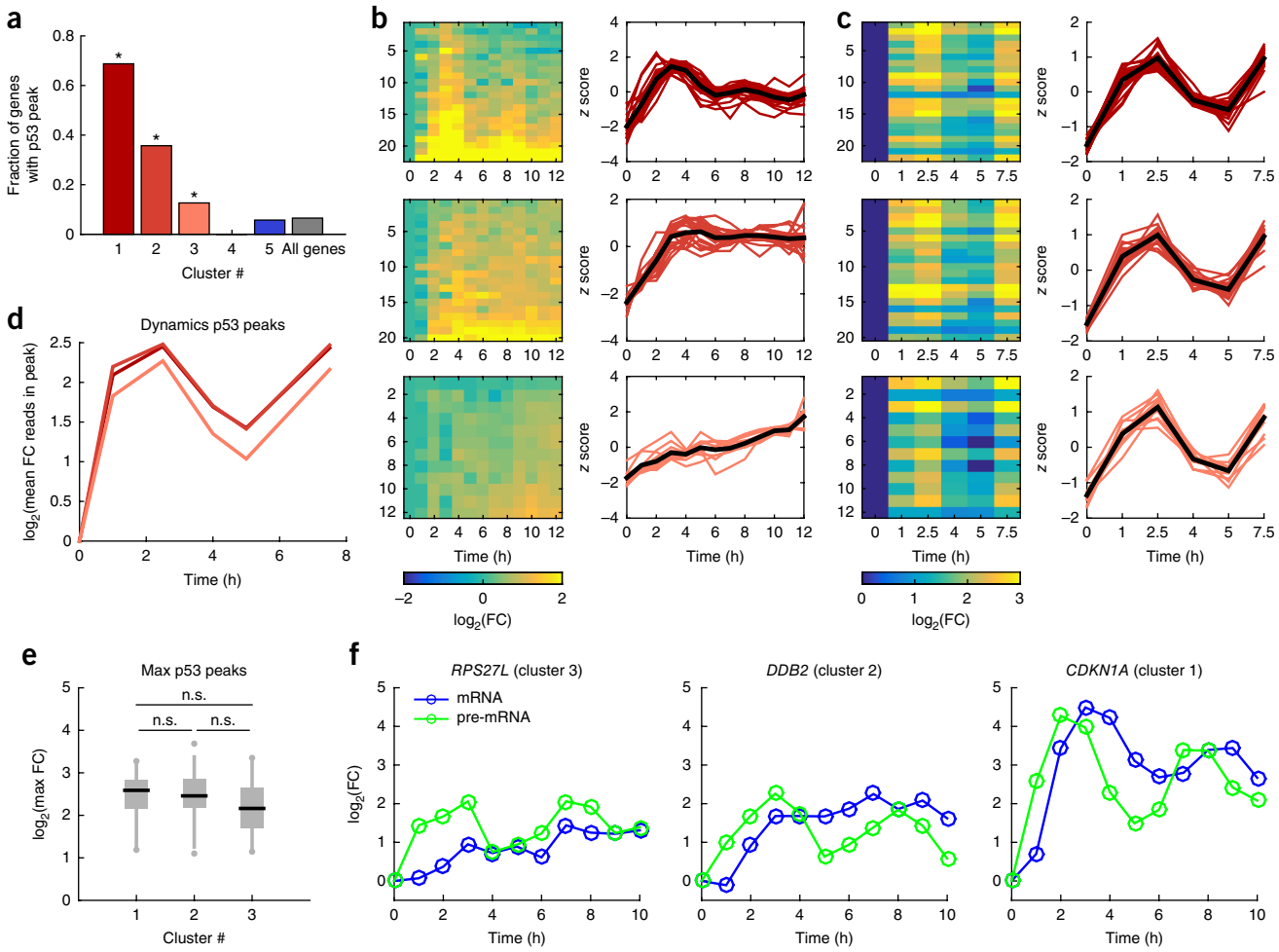

Figure 3 p53 target genes with distinct expression dynamics show similar dynamics of p53 binding. (**a**) Fraction of genes in each of the five gene expression clusters (**Fig. 1**) with a p53 peak within 20 kb of the TSS. *P* values were calculated using the binomial statistic; * for $P < 0.01$ probability of containing a peak. (**b**) Gene expression dynamics of the induced genes that contain a p53 peak within 20 kb of the TSS with $\log_2$(FC) on the left and normalized expression (*z* scores) on the right. FC, fold change. (**c**) Heat map of p53 ChIP $\log_2$ (fold change) of peaks corresponding to genes in **b** on the left and corresponding *z* scores of the p53 ChIP signal on the right. (**d**) Log_2(fold change) of mean p53 ChIP dynamics per cluster. (**e**) Distribution of maximal fold change of p53 peaks per cluster. Black lines indicate the median, and box edges and whiskers extend to the 25–75% and 5–95% quantiles, respectively. A two-sided *t* test was done to evaluate significance; ns stands for not significant ($P > 0.2$ for all comparisons). (**f**) Quantitative RT-PCR on *CDKN1A*, *DDB2* and *RPS27L* genes, in clusters 1, 2 and 3, respectively, using primers specific for pre-mRNA (green) and mRNA (blue) and averaged over two independent experiments.

in 86.6% of the peaks (compared to 1.5% of background genomic regions) and distributed around the peak center (**Fig. 2d** (HOMER motif, $P = 10^{-2119}$) and **e**). To determine whether p53 shows different binding dynamics at different genomic locations, as suggested by the distinct clusters of gene expression (**Fig. 1b**,**c**), we quantified the ChIP signal over time for all peaks. We observed pulsatile dynamics of p53 ChIP for all genomic sites (**Fig. 2f**,**g**). We tested whether p53 pulses cause global chromatin changes by performing H3K27ac ChIP and found a total of 27,228 peaks (**Supplementary Data Set 2**). Only the peaks that overlapped with p53 peaks (4%) showed pulsatile dynamics (**Fig. 2h**), thus suggesting that the pulsatile ChIP dynamics are specific to p53.

Taken together, our data showed that in response to γ-irradiation, pulses of p53 protein levels are converted into pulses of p53 DNA binding across the genome. This suggests that the differential expression patterns we observed at the mRNA level (**Fig. 1**) do not result from distinct binding dynamics at different loci but rather from other mechanisms.

p53 target genes with different dynamics show similar p53 binding

To directly associate p53 binding with gene expression, we assigned each peak to the closest gene and imposed a distance cutoff of 20 kb from the transcription start site (TSS). Cluster 1 was the most enriched in p53-bound genes; 69% of genes in this cluster had a p53 peak (binomial statistic, $P < 1 \times 10^{-16}$, **Fig. 3a**). The other two activated clusters also showed enrichment in p53-bound genes, with 36% of genes in cluster 2 ($P = 1.8 \times 10^{-11}$) and 13% in cluster 3 ($P = 0.01$). Cluster 5 had <10% of genes that were bound by p53 (not significant, $P = 0.4$). The small fraction of differentially repressed genes that are bound by p53 is consistent with previous studies suggesting that p53 does not directly act as a repressor of transcription[22,31–33]. In agreement with our p53 shRNA data (**Fig. 1e** and **Supplementary Fig. 1a**), there were no p53 ChIP peaks in cluster 4.

We next focused on p53-bound genes in clusters 1, 2 and 3. Note that the expression levels of all p53-bound genes in these

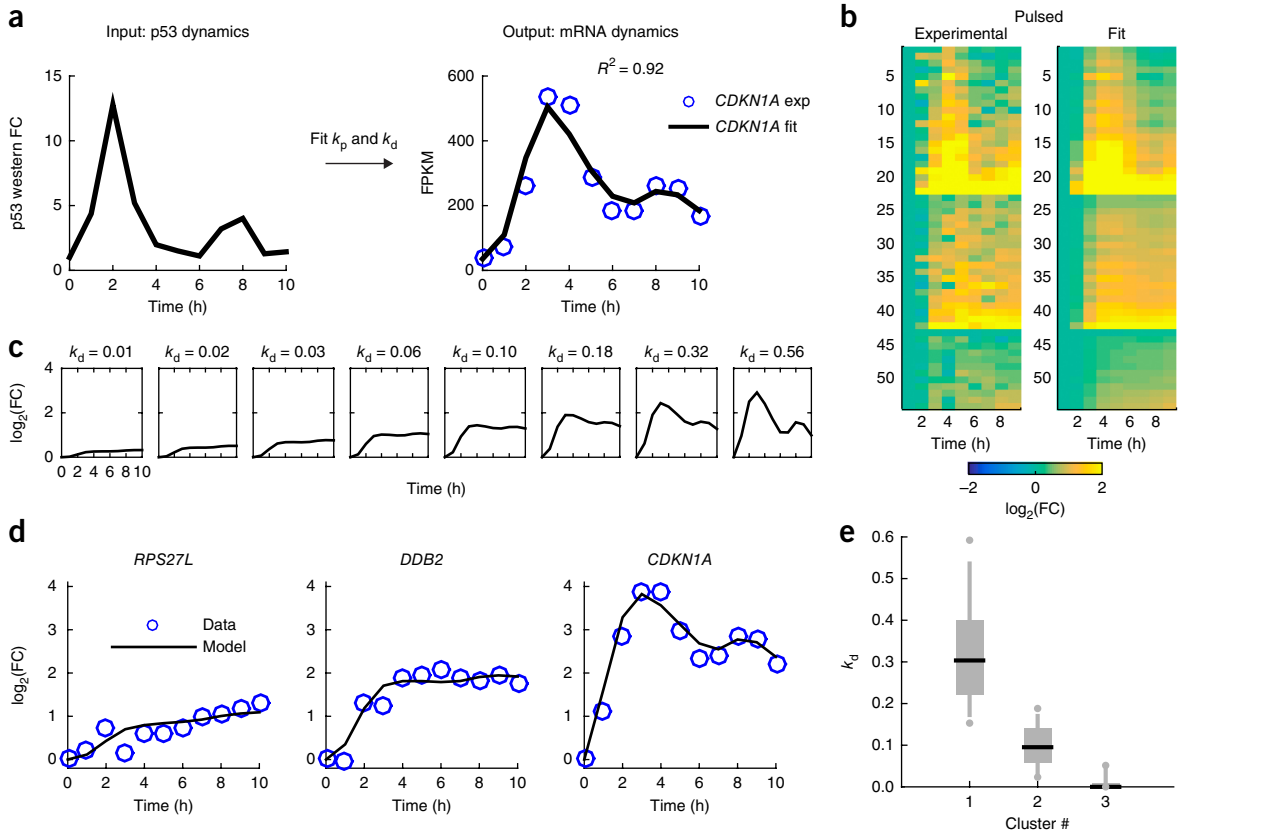

Figure 4 Mathematical model links the input–output relationship between p53 protein dynamics and the dynamics of its target genes genome wide. (**a**) Using p53 protein dynamics (quantified from **Fig. 1a**) as the input, we fit the production and degradation rates, k_p and k_d, respectively, to the mRNA-seq data. The results for the *CDKN1A* gene is shown as an example. FPKM, fragments per kilobase of transcript per million mapped reads. FC, fold change. (**b**) Heatmap of mRNA-seq data of p53 target genes (same as **Fig. 3b**) and corresponding fit data from the model. (**c**) Model simulation varying only the k_d parameter. (**d**) Examples of mRNA-seq measurements (blue circles) and model (black lines) of three genes from clusters 1 (*CDKN1A*), 2 (*DDB2*), and 3 (*RPS27L*). (**e**) Distributions of k_d values per cluster. Black lines indicate the median, and box edges and whiskers extend to the 25–75% and 5–95% quantiles, respectively. Individual dots represent outliers.

clusters were significantly lower in the p53 shRNA cell line relative to wild-type cells, consistent with these genes being direct targets of p53. We determined the quantitative differences in p53 binding to genes in these clusters by plotting the average ChIP signal for each cluster over time after irradiation. Surprisingly, we found that the three activated clusters, which showed distinct mRNA dynamics, had similar dynamics of p53 binding (**Fig. 3b**,**c**). In addition, no significant difference was observed in the fold changes or absolute ChIP peak signals among clusters (**Fig. 3d**,**e** and **Supplementary Fig. 2**). The observation that p53 binds similarly to all induced genes suggests that the distinct dynamics of p53 target genes do not result from distinct binding but from either additional regulation of transcription (for example, p53 cofactors) or post-transcriptional mechanisms. To distinguish between these two possibilities, we measured the pre-mRNA dynamics of three p53 target genes representative of the three clusters with distinct mRNA dynamics. We found similar pre-mRNA pulsatile profiles albeit distinct mature mRNA dynamics (**Fig. 3f**), thus suggesting that post-transcriptional mechanisms contribute to the differential dynamics observed between clusters.

The dynamics of p53-dependent target genes are determined by their mRNA half-lives

How can pulsatile p53 give rise to different mRNA dynamics despite similar DNA binding and transcription? To answer this, we built a two-parameter model describing mRNA dynamics with p53 protein levels as input:

$$\frac{\mathrm{dmRNA}(t)}{\mathrm{d}t} = k_p \times \mathrm{p53}(t-1) - k_\mathrm{d} \times \mathrm{mRNA}(t) \qquad (1)$$

We used p53 levels at $t-1$ h as the input for p53 (**Fig. 1a**, quantified in **4a**) and fit the production and degradation rate constants, k_p and k_d, respectively, to the measured mRNA-seq data of p53-bound induced genes (Online Methods and **Supplementary Data Set 3**). We obtained a fit with $R^2 = 0.92$ for the *CDKN1A* gene (**Fig. 4a**) and a median $R^2 = 0.75$ for all genes compared to $R^2 = 0.46$ for genes without a p53 peak (**Fig. 4b**, **Supplementary Fig. 3a**, Wilcoxon rank-sum test $P = 2.23 \times 10^{-7}$).

The activation rate k_p showed a significant correlation with the maximal p53 ChIP peak amplitude on a per-gene basis (Spearman's $\rho = 0.54$, $P = 3.7 \times 10^{-5}$, **Supplementary Fig. 3b**). The k_d was significantly correlated with previously published mRNA half-life data collected in the same cell line[34] (Spearman's $\rho = 0.55$, $P = 8.4 \times 10^{-4}$, **Supplementary Fig. 3c**). The significant correlations between parameters extracted from our model and independent data sets (p53 ChIP and mRNA half-life) further validate the model and suggest that our mathematical formulation can be used to explain p53-dependent gene expression.

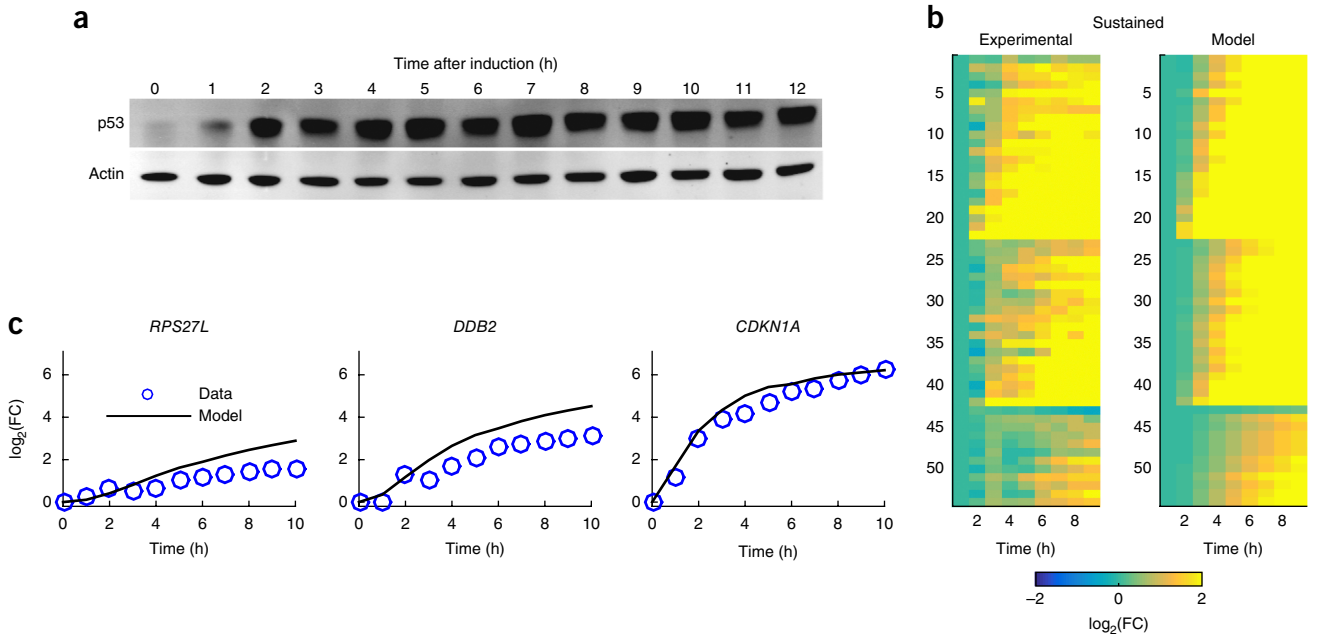

Figure 5 Mathematical model can predict gene expression for sustained p53 input dynamics. (**a**) Western blot for the sustained-p53 condition. Data is representative of three independent experiments (uncropped gel image shown in **Supplementary Data Set 5**). (**b**) Using sustained p53 protein dynamics derived from **a**, and k_p and k_d derived from the pulsed data, gene expression can be predicted under the sustained-p53 condition. Results are shown as a heat map for experimental data and model prediction. FC, fold change. (**c**) Examples of model prediction and mRNA measurements for the *RPS27L*, *DDB2* and *CDKN1A* genes.

We ran a simulation for a range of k_p and k_d parameters to explore their contribution to specific dynamical properties of gene expression (defined in **Supplementary Fig. 3d**). We observed that the maximal induction of gene expression increased with increasing k_p values (**Supplementary Fig. 3e**). This dependency was lost when we looked at the maximal fold change, which was only dependent on the k_d (**Supplementary Fig. 3f**). The k_d also determined the pulsatility and the time to maximal induction, with higher degradation rates leading to pulsatile behavior and faster induction (**Supplementary Fig. 3g,h**). Our simulation therefore suggests that p53 DNA-binding strength determines how strongly a gene is induced; however, the dynamics and timing of activation are controlled through mRNA half-life. In this scenario, different dynamics of target genes in response to p53 pulses can be achieved by solely varying the k_d values while maintaining constant k_p (**Fig. 4c**). Indeed, the three genes representative of the three expression clusters with pulsatile pre-mRNA (**Fig. 3f**) had different k_d values (**Fig. 4d**). At the global level, genes in cluster 1 had higher k_d values compared to genes in clusters 2 and 3 ($P < 1 \times 10^{-5}$, Wilcoxon rank-sum test, **Fig. 4e**).

A mathematical model can predict the dynamics of p53-dependent genes under different p53 dynamical inputs

Can our model of gene regulation by p53 (equation 1) be applied for a different dynamical input? To test the predictive power of the model, we perturbed p53 dynamics from pulses to sustained expression using an established protocol[3] (**Fig. 5a**) and used the parameters derived from the pulsed condition to predict mRNA dynamics under the sustained condition. The predicted mRNA dynamics for p53 target genes were in strong agreement with the levels measured by mRNA-seq (median $R^2 = 0.91$ versus $R^2 = 0.72$ for genes without a p53 peak, Wilcoxon rank-sum test $P = 2.27 \times 10^{-7}$, **Fig. 5b,c** and **Supplementary Fig. 3i,j** and **Supplementary Data Set 4**). Thus, the k_p and k_d parameters that were derived from the pulsed condition can predict the expression of target genes under different p53 input dynamics.

DISCUSSION

How transcription factor dynamics affect the dynamics of their target genes is a fundamentally important question. Here, we focused on the stereotypic pulses of the transcription factor protein p53 and sought to determine how different target genes respond to variations in its dynamics. Using high-temporal resolution mRNA-seq, we identified three clusters of p53-dependent induced genes, with distinct gene expression dynamics: pulses, induction and a plateau, or continuous accumulation. However, when we measured the dynamics of p53 binding to its target genes using ChIP-seq, we observed pulsatile dynamics genome wide. Thus, p53 pulses were translated into pulsatile DNA binding but were not predictive of the output gene expression. We used mathematical modeling to understand how a uniform pulsatile input can give rise to different dynamics of gene expression. Using a two-parameter model with p53 protein levels as input, we found that we can recapitulate the different activation dynamics of p53 target genes. Moreover, our model parameters provide a mechanistic understanding of gene regulation by p53, in which the strength of p53 binding contributes to the maximal induction of gene expression, and the mRNA-degradation rate has an important role in the dynamic pattern of activation. We further used the model to predict gene expression dynamics for sustained p53 input and experimentally validated these predictions across the genome, thus demonstrating that our model can be used to predict gene expression for a new dynamical input of p53.

The contribution of mRNA half-life to the dynamics of gene expression has previously been observed for a subset of p53 target genes[23,24]. Our study, looking at genome-wide mRNA dynamics in a wild-type and p53-knockdown context, as well as integrating gene expression with time course p53 ChIP-seq data, allowed us to identify all p53-dependent and directly bound genes among the differentially expressed genes in response to γ-irradiation and to formulate a general model that explains and predicts mRNA dynamics of these target

genes as a function of p53 input dynamics. We demonstrated the utility of our model for predicting gene expression in response to a different dynamical input of p53. A similar framework can be applied for future studies to determine the input–output relationship between p53 dynamics and its target genes under additional conditions and cellular backgrounds. Analogously to their role in the p53 system, mRNA half-lives were also found to be important in tuning the timing and pattern of gene expression in response to NF-κB oscillations[35,36]. Further studies are required to determine whether a similar general model of gene regulation could be used to predict expression of NF-κB target genes in response to different NF-κB input dynamics.

How p53 chooses between its target genes is a longstanding fundamental question. Our study suggests that, in the context of DNA damage, p53 itself does not choose which target gene to activate; rather, it globally binds to DNA in a temporal pattern that mimics the dynamics of its protein levels, whereas the degradation rate of mRNA dominates the timing, profile and fold change of gene induction. Although we cannot exclude the contribution of other cofactors to the induction of specific p53 targets, our global observations are in agreement with a recent study, which used a high-throughput enhancer assay to test p53-bound genomic regions and determined that p53 can act in isolation[22].

Lastly, our study provides new insights into the question of why p53 pulses in response to DNA damage. Expression dynamics of genes with short mRNA half-life, for example *CDKN1A*, follow p53 protein dynamics and thus have different dynamics under pulsed and sustained p53 inputs (**Figs. 4d** and **5c**). On the other hand, genes with long mRNA half-lives, like *RPS27L*, low-pass filter the p53 signal and act as integrators (**Figs. 4d** and **5c**). Different effectors of p53 signaling may therefore act as integrators or instantaneous readouts of p53 activity. In addition, under sustained p53 levels, gene expression dynamics show continuous accumulation and are less variable between genes (**Fig. 5b**,**c** and **Supplementary Fig. 3j**). On a global scale, sustained p53 dynamics result in a more uniform pattern of gene expression than does pulsatile p53 input, with significantly smaller Euclidean distances between genes in different clusters (**Supplementary Table 1**). These findings suggest that p53 pulses may provide a mechanism for diverse gene expression patterns that cannot be achieved under sustained-input conditions. Future studies are required for understanding why p53 target genes in the different clusters have different mRNA half-lives and the molecular mechanisms that control this differential mRNA stability. In addition, the impact of mRNA half-life on protein levels, and consequently on cell fate decision in response to different p53 inputs, remains an important open direction for future investigation.

METHODS

Methods, including statements of data availability and any associated accession codes and references, are available in the online version of the paper.

Note: Any Supplementary Information and Source Data files are available in the online version of the paper.

ACKNOWLEDGMENTS

We thank S. Boswell for help with RNA-seq experiments and X. Zhang (Broad Institute) for help with p53 ChIP experiments, M. Springer for helpful discussions and advice on modeling, and members of the Lahav lab for comments and discussion. This research was supported by Novartis Institutes for Biomedical Research and NIH grant GM083303. A.H. was supported by Boehringer Ingelheim Fonds, PhD fellowship. J.S.-O. was supported by NIH grant CA207727. J.E.P. was supported by NIH grant GM102372. M.L.B. was supported by NIH grant HG003985.

AUTHOR CONTRIBUTIONS

A.H., J.E.P., W.C.F. and G.L. conceived experiments. A.H., M.L.B. and G.L. conceived analyses. A.H. performed experiments and A.H. and J.S.-O. performed analyses. A.H. and G.L. wrote the paper.

COMPETING FINANCIAL INTERESTS

The authors declare no competing financial interests.

1. Cai, L., Dalal, C.K. & Elowitz, M.B. Frequency-modulated nuclear localization bursts coordinate gene regulation. *Nature* **455**, 485–490 (2008).
2. Hoffmann, A., Levchenko, A., Scott, M.L. & Baltimore, D. The IkappaB-NF-kappaB signaling module: temporal control and selective gene activation. *Science* **298**, 1241–1245 (2002).
3. Purvis, J.E. *et al.* p53 dynamics control cell fate. *Science* **336**, 1440–1444 (2012).
4. Paek, A.L., Liu, J.C., Loewer, A., Forrester, W.C. & Lahav, G. Cell-to-cell variation in p53 dynamics leads to fractional killing. *Cell* **165**, 631–642 (2016).
5. Hao, N. & O'Shea, E.K. Signal-dependent dynamics of transcription factor translocation controls gene expression. *Nat. Struct. Mol. Biol.* **19**, 31–39 (2011).
6. Covert, M.W., Leung, T.H., Gaston, J.E. & Baltimore, D. Achieving stability of lipopolysaccharide-induced NF-kappaB activation. *Science* **309**, 1854–1857 (2005).
7. Batchelor, E., Loewer, A., Mock, C. & Lahav, G. Stimulus-dependent dynamics of p53 in single cells. *Mol. Syst. Biol.* **7**, 488 (2011).
8. Hansen, A.S. & O'Shea, E.K. Encoding four gene expression programs in the activation dynamics of a single transcription factor. *Curr. Biol.* **26**, R269–R271 (2016).
9. Werner, S.L., Barken, D. & Hoffmann, A. Stimulus specificity of gene expression programs determined by temporal control of IKK activity. *Science* **309**, 1857–1861 (2005).
10. Lahav, G. *et al.* Dynamics of the p53-Mdm2 feedback loop in individual cells. *Nat. Genet.* **36**, 147–150 (2004).
11. Lev Bar-Or, R. *et al.* Generation of oscillations by the p53-Mdm2 feedback loop: a theoretical and experimental study. *Proc. Natl. Acad. Sci. USA* **97**, 11250–11255 (2000).
12. Weinberg, R.L., Veprintsev, D.B., Bycroft, M. & Fersht, A.R. Comparative binding of p53 to its promoter and DNA recognition elements. *J. Mol. Biol.* **348**, 589–596 (2005).
13. Qian, H., Wang, T., Naumovski, L., Lopez, C.D. & Brachmann, R.K. Groups of p53 target genes involved in specific p53 downstream effects cluster into different classes of DNA binding sites. *Oncogene* **21**, 7901–7911 (2002).
14. Kracikova, M., Akiri, G., George, A., Sachidanandam, R. & Aaronson, S.A. A threshold mechanism mediates p53 cell fate decision between growth arrest and apoptosis. *Cell Death Differ.* **20**, 576–588 (2013).
15. Murray-Zmijewski, F., Slee, E.A. & Lu, X. A complex barcode underlies the heterogeneous response of p53 to stress. *Nat. Rev. Mol. Cell Biol.* **9**, 702–712 (2008).
16. Flores, E.R. *et al.* p63 and p73 are required for p53-dependent apoptosis in response to DNA damage. *Nature* **416**, 560–564 (2002).
17. Samuels-Lev, Y. *et al.* ASPP proteins specifically stimulate the apoptotic function of p53. *Mol. Cell* **8**, 781–794 (2001).
18. Oda, K. *et al.* p53AIP1, a potential mediator of p53-dependent apoptosis, and its regulation by Ser-46-phosphorylated p53. *Cell* **102**, 849–862 (2000).
19. Smeenk, L. *et al.* Role of p53 serine 46 in p53 target gene regulation. *PLoS One* **6**, e17574 (2011).
20. Sykes, S.M. *et al.* Acetylation of the p53 DNA-binding domain regulates apoptosis induction. *Mol. Cell* **24**, 841–851 (2006).
21. Nikulenkov, F. *et al.* Insights into p53 transcriptional function via genome-wide chromatin occupancy and gene expression analysis. *Cell Death Differ.* **19**, 1992–2002 (2012).
22. Verfaillie, A. *et al.* Multiplex enhancer-reporter assays uncover unsophisticated TP53 enhancer logic. *Genome Res.* **26**, 882–895 (2016).
23. Porter, J.R., Fisher, B.E. & Batchelor, E. p53 pulses diversify target gene expression dynamics in an mRNA half-life-dependent manner and delineate co-regulated target gene subnetworks. *Cell Syst.* **2**, 272–282 (2016).
24. Melanson, B.D. *et al.* The role of mRNA decay in p53-induced gene expression. *RNA* **17**, 2222–2234 (2011).
25. Batchelor, E., Mock, C.S., Bhan, I., Loewer, A. & Lahav, G. Recurrent initiation: a mechanism for triggering p53 pulses in response to DNA damage. *Mol. Cell* **30**, 277–289 (2008).
26. Wei, C.L. *et al.* A global map of p53 transcription-factor binding sites in the human genome. *Cell* **124**, 207–219 (2006).
27. El-Deiry, W.S. *et al.* WAF1, a potential mediator of p53 tumor suppression. *Cell* **75**, 817–825 (1993).
28. Botcheva, K., McCorkle, S.R., McCombie, W.R., Dunn, J.J. & Anderson, C.W. Distinct p53 genomic binding patterns in normal and cancer-derived human cells. *Cell Cycle* **10**, 4237–4249 (2011).

29. El-Deiry, W.S., Kern, S.E., Pietenpol, J.A., Kinzler, K.W. & Vogelstein, B. Definition of a consensus binding site for p53. *Nat. Genet.* **1**, 45–49 (1992).
30. Riley, T., Sontag, E., Chen, P. & Levine, A. Transcriptional control of human p53-regulated genes. *Nat. Rev. Mol. Cell Biol.* **9**, 402–412 (2008).
31. Fischer, M., Steiner, L. & Engeland, K. The transcription factor p53: not a repressor, solely an activator. *Cell Cycle* **13**, 3037–3058 (2014).
32. Schlereth, K. *et al.* Characterization of the p53 cistrome–DNA binding cooperativity dissects p53's tumor suppressor functions. *PLoS Genet.* **9**, e1003726 (2013).
33. Rashi-Elkeles, S. *et al.* Parallel profiling of the transcriptome, cistrome, and epigenome in the cellular response to ionizing radiation. *Sci. Signal.* **7**, rs3 (2014).
34. Schueler, M. *et al.* Differential protein occupancy profiling of the mRNA transcriptome. *Genome Biol.* **15**, R15 (2014).
35. Zambrano, S., De Toma, I., Piffer, A., Bianchi, M.E. & Agresti, A. NF-κB oscillations translate into functionally related patterns of gene expression. *eLife* **5**, e09100 (2016).
36. Hao, S. & Baltimore, D. The stability of mRNA influences the temporal order of the induction of genes encoding inflammatory molecules. *Nat. Immunol.* **10**, 281–288 (2009).

ONLINE METHODS

Cell culture and DNA damage treatment. MCF7 + p53 shRNA, from the Agami group[37], and MCF7 cells were grown in RPMI + 10% FBS supplemented with 100 mL/L FBS, 100 U/mL penicillin, 100 mg/mL streptomycin, and 250 ng/mL fungizone (Gemini Bio-Products). The identity of MCF7 and MCF7 p53shRNA cell lines was confirmed by DNA fingerprinting with small tandem repeat profiling. MCF7 tested negatively for mycoplasma contamination. Irradiation and irradiation with Nutlin 3a treatment, for the sustained p53 dynamics were performed as described in ref. 3.

RNA-seq. RNA was collected using TRIZOL reagent and purified using the Zymo RNA Clean-up kit. 500 ng of RNA was used as input for the Illumina TruSeq Stranded mRNA Library Prep Kit. Barcoded libraries were pooled and single-end sequenced on Illumina Next-Seq.

ChIP-seq. MCF7 cells were cross-linked in 1% formaldehyde for 5 min at room temperature, quenched with glycine, and washed in ice-cold PBS with protease inhibitors (Roche). Pellets were flash frozen in liquid nitrogen and stored at −80 °C. Cross-linked cells were thawed on ice and lysed for 10 min in ice-cold lysis buffer (10 mM Tris-HCl, pH 8.0, 10 mM NaCl, 0.5% NP-40 with protease inhibitors (Roche) and 500 μM DTT added just before use). Following a 5-min spin, pellets were washed in ice-cold 1× PBS, followed by a second 5-min spin, after which the supernatant was discarded and nuclei were lysed for 10 min in nuclei lysis buffer (50 mM Tris-HCl, pH 8.0, 10 mM EDTA, 0.32% SDS) and sonicated using Diagenode Bioruptor for 15 min using high power and a 30-s-on, 30-s-off cycle. The remainder of the ChIP protocol was done according to the Broad ChIP Protocol from the Roadmap Epigenomics project (http://www.roadmapepigenomics.com) using 5 million cells, 3 μl of X-DO1 (Santa Cruz, sc-126 X) anti-p53 antibody and anti-H3K27ac antibody (Abcam, ab4729). Illumina library preparation was done using the Nugen Ovation Ultralow Library Systems V2 kit. Barcoded libraries were pooled and sequenced on Illumina Next-Seq. For p53 ChIP, cells were cross-linked at the following time points post irradiation: 0 h, 1 h, 2.5 h, 5 h and 7.5 h. For H3K27ac ChIP and ChIP input samples, the following time points were used: 0 h, 2.5 h, 5 h and 7.5 h.

Quantitative RT-PCR. The same RNA samples used for RNA-seq were used to generate complementary DNA using the high-capacity cDNA reverse transcription protocol (Applied Biosystems). Quantitative RT-PCR was then performed using 10 ng of cDNA, 100 nM primer, and SYBR Green reagent (Applied Biosystems). Normalization was done to the average of both ACTB and GAPDH genes.

qPCR primers used: CDKN1A mRNA (F: TGTCACTGTCTTGTACCCTTG, R: GGCGTTTGGAGTGGTAGAA); CDKN1A pre-mRNA (F: CCCGGCC AGGTAACATAGT, R: CATGGGTTCTGACGGACATC); DDB2 mRNA (F: TCGTCAGGACCCTCCAC, R: CGCCAAGGATGTAGCCC); DDB2 intron (F: CGCTAGAGTGCAGTGATTCG, R: GGTGGTAGGTGCATGTGGTT); RPS27L mRNA (F: CGTCCTTGGAAGAGGAAAAG,

R: ACCGTGGTGATCTTGTAGCA); RPS27L pre-mRNA (F: GGGATTGC TAGTGTGGTGTG, R: TGTCCCTGACATTTCCAATTC); GAPDH (F: ACAT CGCTCAGACACCATG, R: TGTAGTTGAGGTCAATGAAGGG); ACTB

(F: ACCTTCTACAATGAGCTGCG, R: CCTGGATAGCAACGTACATGG).

RNA-seq data analysis. RNA-seq reads were mapped and analyzed by TopHat and Cufflinks RNA-seq analysis pipeline[38], using Tophat version 2.1.0 and Cufflinks version 2.1.1. Alignment was done against the hg19 genome, and hg19 RefSeq.gtf transcript annotations were used.

Selection of differentially expressed genes was done by calculating the fold change and significance relative to basal expression on the two biological replicates and selecting the genes that show a fold change above 2 with FDR (Benjamini–Hochberg) below 0.2 at any time point. Clustering was done on z scores using Fuzzy c-means clustering with an exponent for the fuzzy partition matrix of 1.3 and five clusters. Small variation in parameter values does not qualitatively affect the results and their interpretation.

We also performed a parallel analysis, selecting genes that were significantly different between wild-type and p53sh conditions. To be called significantly different, a gene had to pass at least one of two criteria: (1) the difference in fold change per time point between wild-type and p53sh had to be significantly different from zero using a Wilcoxon signed-rank test and $P < 0.05$, or (2) the dynamics of expression between wild-type and p53sh had to be uncorrelated (Spearman and $P > 0.05$). The expression of 92.6% of the genes presented in **Figure 1** were significantly affected upon p53 knockdown. Clustering these genes, on the basis of their fold change in expression in the p53 wild-type cell line, led to four clusters with clusters 1, 2, 3 and 5 remaining largely unchanged and retaining their cluster identity. Cluster 4 disappeared and the remaining p53-dependent genes in this cluster were assigned to clusters 3 and 5.

GO Enrichment analysis was done using Enrichr software[39,40].

ChIP-seq data analysis. Reads were aligned to the human reference genome (hg19) using the Bowtie 1 algorithm and only uniquely aligned reads were retained[41]. Duplicate reads were removed for downstream analyses. For peak calling, the IDR framework[42,43] with the MACS2 (ref. 44) algorithm was used. Briefly, reads from all time points were pooled together and peaks were called using the MACS2 software using $P = 1 \times 10^{-3}$ as a cutoff on the pooled reads file and on pseudo-replicate files in which reads from the pooled file were randomly split in half. We identified 4,141 peaks with a 0.0025 IDR threshold. For these 4,141 peaks, we defined regions of + and − 300 bp around the peak center to count the number of reads per peak for each condition, which were then normalized to the total number of reads in the sample. For the analysis looking at p53 peak amplitude, the average number of input reads over all time points and mapping to the corresponding peak locations was subtracted from the p53 ChIP reads.

The HOMER package[45] was used for *de novo*–motif discovery. WebLogo was used to generate the motif plot[46] in **Figure 2** for the top enriched motif. The top enriched motif (**Fig. 2**) was then used to rescan and score all peaks and background regions. Background regions were generated by selecting 600-bp regions adjacent to either side of the peak and excluding regions that overlap with p53 peak regions.

Mapping of peaks to genes was done using the HOMER package to find the closest gene. Only peaks with 20 kb relative to the TSS of each gene were used for the analyses. For genes with multiple p53 ChIP peaks, the signal from the closest p53 ChIP peak was used.

Model. Because of the discrete time points of our data, we implemented the model in equation (1) by calculating the mRNA level at each step for a given set of k_p and k_d parameters at each time point.

$$m(t) = (1 - k_d)m(t-1) + k_p p53(t-1)$$

Quantification of the p53 western blot (**Fig. 1a**, quantified in **Fig. 4a**) was used as the input for p53 levels for the pulsed condition. For the sustained p53 condition, we quantified the western blot (**Fig. 5a**) and used it as the model input.

We fit the model under the pulsed p53 condition as to minimize the square of the Pearson's correlation between the predicted and the measured mRNA levels for each gene.

Statistical analyses. In the cases in which t tests were used, the Anderson–Darling test was used to test for normality. Binomial statistics were used to calculate P values in **Figure 3a** and **Supplementary Figure 1a**. Wilcoxon signed-rank tests were used for non-normal distributions.

A **Life Sciences Reporting Summary** for this article is available.

Data availability. All sequencing data for ChIP-seq and RNA-seq experiments have been deposited in NCBI's Gene Expression Omnibus and are accessible through GEO Series accession number GSE100099.

FPKM values and $\log_2$(fold change) per time point following γ-irradiation for 229 differentially expressed genes as well as their cluster assignments are available in **Supplementary Data Set 1**. p53 ChIP-seq peaks with their genomic coordinates, corresponding gene assignments and normalized read counts are available in **Supplementary Data Set 2**. H3K27ac ChIP-seq peaks with their genomic coordinates, distance to the closest p53 ChIP peak and normalized read counts are available in **Supplementary Data Set 2**. Fitting parameters for the 54 p53 bound genes in **Figure 4** are provided in **Supplementary Data Set 3**. FPKM values under sustained p53 condition for 54 genes shown in **Figure 5** as well as the result of the model fit are available in **Supplementary Data Set 4**.

Source code for the mathematical model can be made available upon request.

37. Brummelkamp, T.R., Bernards, R. & Agami, R. A system for stable expression of short interfering RNAs in mammalian cells. *Science* **296**, 550–553 (2002).
38. Trapnell, C. *et al.* Differential gene and transcript expression analysis of RNA-seq experiments with TopHat and Cufflinks. *Nat. Protoc.* **7**, 562–578 (2012).
39. Kuleshov, M.V. *et al.* Enrichr: a comprehensive gene set enrichment analysis web server 2016 update. *Nucleic Acids Res.* **44**, W90–W97 (2016).
40. Chen, E.Y. *et al.* Enrichr: interactive and collaborative HTML5 gene list enrichment analysis tool. *BMC Bioinformatics* **14**, 128 (2013).
41. Langmead, B., Trapnell, C., Pop, M. & Salzberg, S.L. Ultrafast and memory-efficient alignment of short DNA sequences to the human genome. *Genome Biol.* **10**, R25 (2009).
42. Li, Q., Brown, J.B., Huang, H. & Bickel, P.J. Measuring reproducibility of high-throughput experiments. *Ann. Appl. Stat.* **5**, 1752–1779 (2011).
43. Landt, S.G. *et al.* ChIP-seq guidelines and practices of the ENCODE and modENCODE consortia. *Genome Res.* **22**, 1813–1831 (2012).
44. Zhang, Y. *et al.* Model-based analysis of ChIP-Seq (MACS). *Genome Biol.* **9**, R137 (2008).
45. Heinz, S. *et al.* Simple combinations of lineage-determining transcription factors prime cis-regulatory elements required for macrophage and B cell identities. *Mol. Cell* **38**, 576–589 (2010).
46. Crooks, G.E., Hon, G., Chandonia, J.M. & Brenner, S.E. WebLogo: a sequence logo generator. *Genome Res.* **14**, 1188–1190 (2004).

doi:10.1038/nsmb.3452

nature research

Corresponding author(s): Galit Lahav

☐ Initial submission ☐ Revised version ☒ Final submission

Life Sciences Reporting Summary

Nature Research wishes to improve the reproducibility of the work that we publish. This form is intended for publication with all accepted life science papers and provides structure for consistency and transparency in reporting. Every life science submission will use this form; some list items might not apply to an individual manuscript, but all fields must be completed for clarity.

For further information on the points included in this form, see Reporting Life Sciences Research. For further information on Nature Research policies, including our data availability policy, see Authors & Referees and the Editorial Policy Checklist.

Experimental design

1. Sample size

Describe how sample size was determined.

Number of time points for RNA-Seq and ChIP-Seq experiments was determined based on the time-scale of p53 pulses and the rationale is describe in text.

2. Data exclusions

Describe any data exclusions.

No data was excluded from analyses.

3. Replication

Describe whether the experimental findings were reliably reproduced.

2 biological replicates were used for RNA-Seq experiment. Both replicates were used for the analysis.

4. Randomization

Describe how samples/organisms/participants were allocated into experimental groups.

Clustering of RNA-Seq data was performed as described in the Methods section.

5. Blinding

Describe whether the investigators were blinded to group allocation during data collection and/or analysis.

All clustering parameters that were used to group gene expression profiles are described in the methods section.

Note: all studies involving animals and/or human research participants must disclose whether blinding and randomization were used.

6. Statistical parameters

For all figures and tables that use statistical methods, confirm that the following items are present in relevant figure legends (or in the Methods section if additional space is needed).

n/a	Confirmed
☐	☒ The exact sample size (*n*) for each experimental group/condition, given as a discrete number and unit of measurement (animals, litters, cultures, etc.)
☐	☒ A description of how samples were collected, noting whether measurements were taken from distinct samples or whether the same sample was measured repeatedly
☐	☒ A statement indicating how many times each experiment was replicated
☐	☒ The statistical test(s) used and whether they are one- or two-sided (note: only common tests should be described solely by name; more complex techniques should be described in the Methods section)
☐	☒ A description of any assumptions or corrections, such as an adjustment for multiple comparisons
☐	☒ The test results (e.g. *P* values) given as exact values whenever possible and with confidence intervals noted
☐	☒ A clear description of statistics including central tendency (e.g. median, mean) and variation (e.g. standard deviation, interquartile range)
☐	☒ Clearly defined error bars

See the web collection on statistics for biologists for further resources and guidance.

Nature Structural & Molecular Biology: doi:10.1038/nsmb.3452

Software

Policy information about availability of computer code

7. Software

Describe the software used to analyze the data in this study.	Public software was used for RNA-Seq and ChIP-Seq analyses (described in the methods section). Custom Matlab code was written for the model and data fitting and can be made available upon request. All parameters and fitting results are provided in the supplemental material.

For manuscripts utilizing custom algorithms or software that are central to the paper but not yet described in the published literature, software must be made available to editors and reviewers upon request. We strongly encourage code deposition in a community repository (e.g. GitHub). *Nature Methods* guidance for providing algorithms and software for publication provides further information on this topic.

Materials and reagents

Policy information about availability of materials

8. Materials availability

Indicate whether there are restrictions on availability of unique materials or if these materials are only available for distribution by a for-profit company.	No unique materials were used

9. Antibodies

Describe the antibodies used and how they were validated for use in the system under study (i.e. assay and species).	The catalog numbers for the antibodies used in this study are provided in the Methods ChIP-Seq section.

10. Eukaryotic cell lines

a. State the source of each eukaryotic cell line used.	MCF7 cell line is the same as used in Lahav et al. 2004 (cited). MCF7-shp53 was obtained from the Agami group (cited).
b. Describe the method of cell line authentication used.	The identity of both MCF7 and MCF7 p53shRNA cell line was confirmed by DNA fingerprinting with small tandem repeat (STR) profiling.
c. Report whether the cell lines were tested for mycoplasma contamination.	Yes, MCF7 cells were screened for mycoplasma contamination.
d. If any of the cell lines used are listed in the database of commonly misidentified cell lines maintained by ICLAC, provide a scientific rationale for their use.	No commonly misidentified cell lines were used.

Animals and human research participants

Policy information about studies involving animals; when reporting animal research, follow the ARRIVE guidelines

11. Description of research animals

Provide details on animals and/or animal-derived materials used in the study.	No animals were used

Policy information about studies involving human research participants

12. Description of human research participants

Describe the covariate-relevant population characteristics of the human research participants.	Did not involve human research participants

Nature Structural & Molecular Biology: doi:10.1038/nsmb.3452

nature research

Corresponding author(s): Galit Lahav

☐ Initial submission ☒ Revised version ☐ Final submission

ChIP-seq Reporting Summary

Form fields will expand as needed. Please do not leave fields blank.

Data deposition

1. For all ChIP-seq data:

☒ a. Confirm that both raw and final processed data have been deposited in a public database such as GEO.

☒ b. Confirm that you have deposited or provided access to graph files (e.g. BED files) for the called peaks.

2. Provide all necessary reviewer access links. *The entry may remain private before publication.*	Submitted to GEO. Link provided in the manuscript.
3. Provide a list of all files available in the database submission.	RNA-Seq Fastq files for 2 biological replicates for: MCF7 10Gy IR, time points 0-12h (at every hour) and 24hrs MCF7 10Gy IR + Nutlin, time points 0-12h (at every hour) and 24hrs MCF7 p53sh RNA 10GY IR, time points 0,2,3,4,5,7,9,10hrs ChIP-Seq data, all in MCF7 cells treated with 10Gy IR. Both raw data in fastq format as well as bedGraph files (for UCSC): p53 ChIP for time points 0,1,2.5,4,5,7.5 hours post IR H3K27ac ChIP for time points: 0,2.5,5,7.5 hours post IR Input ChIP for time points: 0,2.5,5,7.5 hours post IR
4. If available, provide a link to an anonymized genome browser session (e.g. UCSC).	http://genome.ucsc.edu/cgi-bin/hgTracks?hgS_doOtherUser=submit&hgS_otherUserName=toniai&hgS_otherUserSessionName=hg19_Hafner_etal_2017

Methodological details

5. Describe the experimental replicates.	Time course experiment with 6 time points.
6. Describe the sequencing depth for each experiment.	Single end reads. Number of reads in each sample: p53 ChIP t0 : 18199771 p53 ChIP t1 : 31174624 p53 ChIP t2.5 : 28849376 p53 ChIP t4 : 31914329 p53 ChIP t5 : 30311015 p53 ChIP t7.5 : 35041436 H3K27ac ChIP t0: 14996861 H3K27ac ChIP t2.5: 23767268 H3K27ac ChIP t5: 27318093 H3K27ac ChIP t7.5: 27031115 Input t0: 31432250 Input t2.5: 46346817 Input t5: 27981472 Input t7.5: 31847871
7. Describe the antibodies used for the ChIP-seq experiments.	p53 ChIP: Santa Cruz, sc-126 X H3K27ac ChIP: Abcam ab4729

Nature Structural & Molecular Biology: doi:10.1038/nsmb.3452

8. Describe the peak calling parameters.	Peaks were called using a combination of MACS2 and the IDR pipeline as described in the methods section.
9. Describe the methods used to ensure data quality.	IDR pipeline was used to set the peak calling threshold. We verified the existence of known p53 peaks from other studies and ensured the presence of the p53 PWM in the center of the peaks as described in the main text.
10. Describe the software used to collect and analyze the ChIP-seq data.	Genome alignment was done using Bowtie 1. Peak calling was done using MACS2 and IDR pipelines as described in the methods section.

Nature Structural & Molecular Biology: doi:10.1038/nsmb.3452